

Time-reversibility during the aging of materials

Till Böhmer,¹ Jan P. Gabriel,² Jan-Niklas Kociok,¹ Tina Hecksher,² Jeppe C. Dyre,² and Thomas Blochowicz¹

¹*Institute for Condensed Matter Physics, Technical University of Darmstadt, D-64289 Darmstadt, Germany*

²*Glass and Time, IMFUFA, Department of Science and Environment,
Roskilde University, P. O. Box 260, DK-4000 Roskilde, Denmark*

(Dated: 14. April 2023)

Physical aging is the generic term for irreversible processes in glassy materials resulting from molecular rearrangements. We present multi-speckle dynamic light-scattering data on an aging sample of the molecular glass former 1-phenyl-1-propanol following temperature jumps close to the glass transition, starting from and ending in thermal equilibrium. It is demonstrated that the material time of the Tool-Narayanaswamy aging formalism can be determined from the time-autocorrelation function of the scattered-light intensity fluctuations. These fluctuations are shown to be stationary and reversible when regarded as a function of the material time. The glass-forming colloidal synthetic clay Laponite, as well as a chemically aging curing epoxy, are shown also to have material-time-reversible scattered-light intensity fluctuations. Our findings, besides showing direct measurements of the material time, identify a fundamental property of aging in quite different contexts, which presents a challenge to the current theories of aging.

I. INTRODUCTION

Few persons would claim that time can be reversed – all living creatures age and eventually die, a dropped glass breaks while the reverse never happens, mixing cold and warm water leads irreversibly to an in-between temperature, etc [1]. On the other hand, the fundamental equation-of-motion laws of nature are all time reversible, e.g., Newton’s laws of classical mechanics, the Schrödinger equation of quantum mechanics, Maxwell’s equations for electromagnetism, and the Einstein equation of gravity and space-time. The irreversibility of everyday life is accounted for by the second law of thermodynamics, which states that the entropy of an isolated system can increase or stay constant but never decrease [2, 3].

When entropy is constant in time, the system in question is in thermal equilibrium. Reflecting the time reversibility of the fundamental laws, thermal-equilibrium fluctuations are statistically time reversible. As shown by Onsager in 1931, this reversibility leads to quantitative relations between coefficients describing small, linear deviations from equilibrium [4]. This paper presents aging data that go much beyond the linear-response regime, but which are shown nevertheless to be statistically reversible when regarded as functions of the so-called material time that controls aging according to the classical Tool-Narayanaswamy (TN) formalism [5, 6]. Our findings, which are from light-scattering experiments on three quite different samples, question the status of aging as a prototype irreversible phenomenon.

II. PHYSICAL AGING

In contrast to degradation involving chemical reactions as in corrosion, physical aging involves changes of material properties that are caused exclusively by molecular rearrangements [7–15]. Non-crystalline materials like ordinary glass [6, 8], polymers [9, 12, 16], and metallic glasses [13, 17, 18], are all subject to physical aging because the glassy state relaxes continuously toward a state of metastable equilibrium [19]. In the vast majority of cases this is too slow to be observed, but in certain cases physical aging results in undesirable property changes. The study of physical aging is important for the application of glassy materials, as well as for optimizing their production. For this reason – and because it remains disputed what controls the rate of physical aging – this research field continues to attract attention [20–25].

The best controlled physical-aging experiments involve a rapid change of temperature starting from a state of (metastable) thermal equilibrium, after which the system’s path toward equilibrium at an “annealing” temperature is monitored by continuously measuring some physical property. The outcome of such a temperature-jump experiment depends significantly on whether an up or a down jump is considered. Comparing up and down jumps to the same temperature, the latter are faster and more stretched in time than up jumps [8, 12]. Even jumps involving just one percent temperature change result in quite different relaxations toward equilibrium, in some cases with more than a decade variation of the average relaxation time. This “asymmetry of approach” means that physical aging is mathematically a highly nonlinear phenomenon [8, 12] because a linear-response description leads to the same relaxation function except for an overall amplitude scaling.

In many experiments physical aging is described well in terms of the so-called material time [8]. This concept was introduced by Narayanaswamy in 1971, who as an engineer at Ford Motor Co. sought the cooling protocol for

generating optimal frozen-in stresses in the production of windshields [6]. The material time may be thought of as time measured on a clock, the rate of which changes as the glass ages. Conceptually, this is analogous to the proper-time concept of the theory of relativity, i.e., the time measured on a clock following a moving observer. The material-time approach to physical aging is termed the TN formalism [8, 12], an equivalent of which was developed a few years later for aging polymers [26]. The striking mathematical simplification of TN is that physical aging becomes *linear* when described in terms of the material time. Thus for all temperature jumps, a given quantity relaxes toward equilibrium following the *same* function of the material time, except for a scaling proportional to the jump magnitude.

Specifically, when the temperature history is parameterized in terms of the material time ξ , the TN formalism describes aging by a linear convolution integral over the temperature-variation history [6, 8, 16]. Using the laboratory time as the parameter instead, the linear limit is only approached extremely close to thermal equilibrium. The fundamental prediction of TN that knowledge of this limit is enough to determine the highly nonlinear aging phenomenon was recently verified in a paper reporting temperature jumps of amplitude down to 10 mK [27].

According to the TN formalism, linear-response theory applies for the material-time development of *average* quantities. Since linear response by the fluctuation-dissipation theorem [3] reflects equilibrium thermal fluctuations, which are time reversible, this suggests that fluctuations monitored during aging are reversible *if regarded as a function of the material time* instead of the laboratory time; here “reversible” means that past and future cannot be distinguished in the statistical properties of the fluctuations. This conjecture is investigated in the present paper. In order to do so it is necessary to measure thermal fluctuations and to determine the material time during aging.

Our main experimental technique is dynamic light scattering (DLS) [28]. Compared to other experimental methods used for probing aging dynamics, like, e.g., dielectric spectroscopy, the DLS setup operates in the time domain. While frequency-domain experiments with few exceptions [29] must average over at least a few sinusoidal cycles during which the aging material may change its properties, time-domain experiments can, at least in principle, access “instantaneous” autocorrelation or response functions, which are well defined even if aging and correlation decay occur on comparable time scales. In our specific case, to determine the material time $\xi(t)$ as a function of the time t , we assume in the TN spirit that the normalized scattered-light intensity time-autocorrelation function is a function of the material-time difference $\xi(t_2) - \xi(t_1)$. As shown below, this leads to predictions that were first discussed in a seminal paper by Cugliandolo and Kurchan from 1994 [30], although that paper did not discuss how an aging system approaches thermal equilibrium.

It is an experimental challenge to obtain reliable thermal-fluctuation time-autocorrelation data during aging because the standard procedure of ensemble averaging by a moving time average cannot be used. We determine the ensemble average for an aging sample by simultaneously measuring thousands of time-autocorrelation functions with a camera by monitoring a multitude of so-called speckles, i.e., the granular interference pattern of the scattered light. From these data we show how to extract the material time. Using standard methods of time-series analysis it is then demonstrated that, when regarded as a function of the material time, the fluctuations are stationary and reversible. These findings for the molecular system 1-phenyl-1-propanol (1P1P) apply also for the colloidal synthetic clay Laponite studied by VV light scattering that, in contrast to the molecular system, does not approach equilibrium within the time of observation. In search for a counterexample we also studied a curing epoxy that ages chemically by gradual polymerization. Surprisingly, this epoxy system also exhibits material-time reversal invariance, so this property is not limited to physically aging systems.

III. EXPERIMENTAL METHODS IN BRIEF

We use depolarized DLS to probe the temporal intensity fluctuations of light scattered at 90° from the aging sample. These fluctuations reflect the orientational dynamics of the molecules, which is quantified through the intensity time-autocorrelation function. In standard equilibrium DLS experiments the latter is determined via a moving time average of the product of two intensities being separated by the fixed time interval Δt , but as mentioned this cannot be done for an aging sample. To get acceptable statistics we perform a *multi-speckle* DLS experiment that probes a large speckle pattern using a CMOS-camera with 10 pictures taken per second, compare Fig. 1 (a). The intensity fluctuations (Fig. 1 (b)) of different speckles are statistically independent so the time-resolved ensemble-averaged intensity time-autocorrelation function $\langle I(t)I(t + \tau) \rangle$ can be determined by averaging over all pixels of the speckle pattern. This is the main idea; more details are given in the Methods section.

Time-resolved multi-speckle light-scattering has been applied for monitoring aging and ultra-slow dynamics of colloidal glasses, gels, and foams, mainly in the diffusing-wave regime [31–35]. So far, time-resolved multi-speckle light-scattering has not been used to monitor nonequilibrium molecular systems. The concept of calculating multi-pixel averages to obtain time-resolved autocorrelations is also used in connection with X-ray photon correlation spectroscopy, e.g., for studying the physical aging of metallic glasses [36–38].

If the intensity of the scattered light at time t at one pixel is denoted by $I(t)$, the normalized intensity time-autocorrelation function is defined by $C(t_1, t_2) \equiv \langle I(t_1)I(t_2) \rangle / (\langle I(t_1) \rangle \langle I(t_2) \rangle) - 1$ in which the angular brackets are

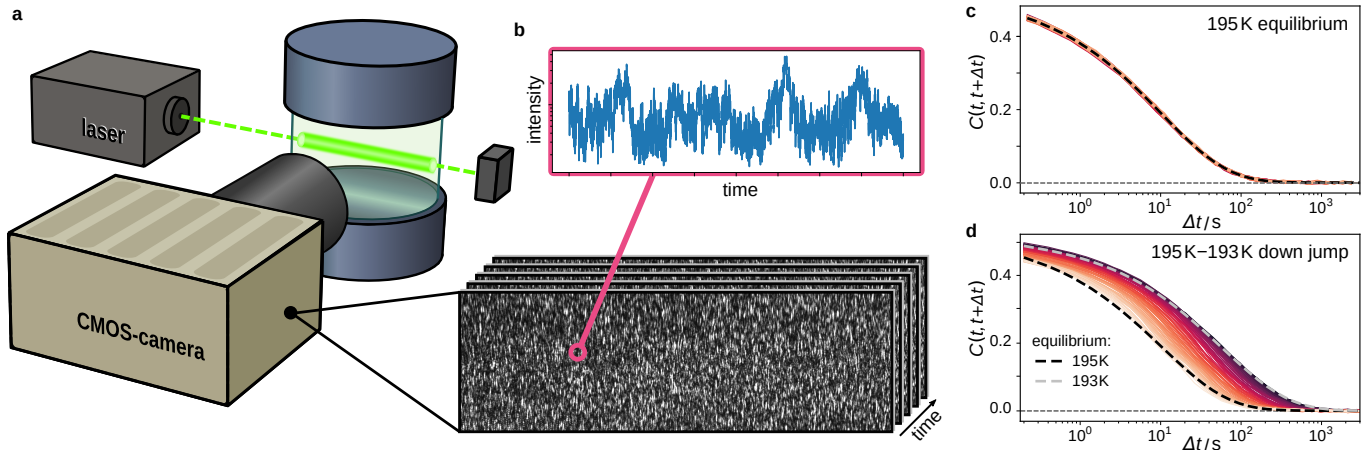


FIG. 1. **Multispeckle dynamic light scattering.** (a) The sample is illuminated by a laser beam and a CMOS-camera is used to detect the speckle pattern of the 90° scattered-light intensity. (b) In each speckle, statistically independent temporal intensity fluctuations are observed. The time-resolved normalized intensity time-autocorrelation function, $C(t, t + \Delta t)$, is obtained as the multi-speckle average. (c) Data for 1-phenyl-1-propanol in thermal equilibrium at 195 K where $C(t, t + \Delta t)$ is stationary, i.e., depends only on Δt . (d) During physical aging following a temperature down jump, $C(t, t + \Delta t)$ changes with t for fixed Δt . The evolution starts from what is the equilibrium time-autocorrelation function at the initial temperature 195 K (left dashed curve) and ends in equilibrium at the annealing temperature 193 K (right dashed curve). The different colors correspond to different times t that are evenly spaced on a logarithmic axis.

averages over the different speckles. The equilibrium supercooled 1P1P normalized intensity time-autocorrelation function $C(t, t + \Delta t)$ is plotted in Fig. 1 (c) as functions of Δt for different times t (different colors). The data collapse onto a single curve, confirming the well-known stationarity of the equilibrium state. In contrast, a distinct t dependence of $C(t, t + \Delta t)$ is observed following a temperature down jump (Fig. 1 (d)). Starting from the initial equilibrium state at 195 K (left dashed curve) the decay of $C(t, t + \Delta t)$ to zero as $\Delta t \rightarrow \infty$ slows down with increasing t . In the figure, darker colors correspond to larger t . Eventually a new stationary equilibrium state is approached at the annealing temperature 193 K (right dashed curve).

IV. IDENTIFYING THE MATERIAL TIME

We determine the material-time as a function of time, $\xi(t)$, from the assumption that the normalized intensity autocorrelation function $C(t_1, t_2)$ reflects the elapsed material time between t_1 and t_2 . In other words, for some monotonous function that goes to zero for $x \rightarrow \infty$, $G(x)$, it is assumed [39] that

$$C(t_1, t_2) = G(\xi(t_2) - \xi(t_1)). \quad (1)$$

For this to apply for any t_1 and t_2 , the following consistency requirement must be obeyed. Since $\xi(t_3) - \xi(t_1) = \xi(t_2) - \xi(t_1) + \xi(t_3) - \xi(t_2)$, $C(t_1, t_3)$ is determined by $C(t_1, t_2)$ and $C(t_2, t_3)$ [40]. This always applies in thermal equilibrium because in that case $C(t_1, t_2)$ is a function of $t_2 - t_1$, which is proportional to $\xi(t_2) - \xi(t_1)$ since ξ in equilibrium is a linear function of time. During aging, however, the consistency requirement is nontrivial as the system's structure changes with time and ξ is no longer a linear function of t .

Introducing the abbreviated notation $C_{12} = C(t_1, t_2)$ etc, the above translates into the so-called triangular relation that was originally derived by Cugliandolo and Kurchan in 1994 in a mean-field calculation of time-autocorrelation functions of infinite-range spin systems quenched from infinite to a low temperature [30],

$$C_{13} = C_{13}(C_{12}, C_{23}). \quad (2)$$

This equation signals that C_{12} and C_{23} uniquely determine C_{13} . Equation (2) describes, in particular, aging following an infinitesimal temperature jump. Equilibrium dynamics is time reversible, implying symmetry of the function C_{13} ,

$$C_{13}(C_{12}, C_{23}) = C_{13}(C_{23}, C_{12}). \quad (3)$$

By the triangular relation this symmetry applies also for an aging sample, a result that was derived by a different argument in Ref. 30.

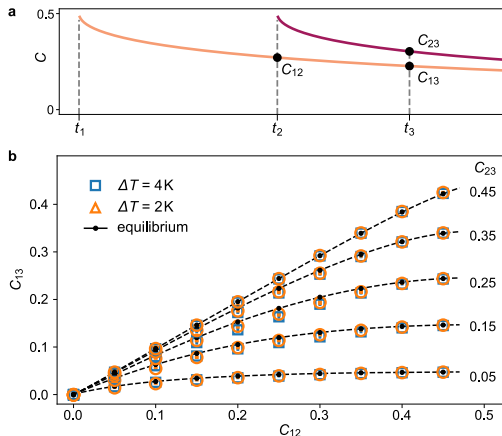


FIG. 2. **Verifying the triangular relation.** (a) Schematic illustration how $C_{12} \equiv C(t_1, t_2)$, C_{13} and C_{23} are defined for $t_1 < t_2 < t_3$. (b) C_{13} plotted vs. C_{12} for fixed values of C_{23} (1P1P data). These data refer to thermal equilibrium at 193 K as well as to physical aging following two temperature down jumps to 193 K. The relation between the three time-autocorrelation functions is the same for the two temperature jumps as in equilibrium. The variations of the C_{13} data are given as error bars. These are smaller than the symbol size (< 0.01), however, making them hard to see. These data confirm the triangular relation Eq. (2), which constitutes a consistency requirement that must be obeyed for using the intensity time-autocorrelation function to define the material time according to Eq. (4).

We checked Eq. (2) by calculating C_{12} , C_{23} , and C_{13} for several million time triplets, $t_1 < t_2 < t_3$, as illustrated in Fig. 2(a). By binning subsets with same C_{12} and C_{23} , we calculated the average C_{13} and its standard deviation σ_{13} . In Fig. 2(b), the average value of C_{13} is plotted as a function of C_{12} for fixed values of C_{23} for 1P1P data measured in equilibrium, as well as after temperature jumps of different magnitude. All data are given with error bars of magnitude σ_{13} that, however, are so small that they are hardly visible. This demonstrates that C_{13} is determined by C_{12} and C_{23} independent of the temperature protocol, thus validating the triangular relation in and out of equilibrium.

Having confirmed a necessary condition for defining the material time via Eq. (1), we note that inverting Eq. (1) leads to for some function $\phi(x)$

$$\xi(t_2) - \xi(t_1) = \phi(C_{12}). \quad (4)$$

Thus, when the normalized intensity time-autocorrelation function has decayed to a certain value, a fixed amount of material time $\Delta\xi$ has elapsed. We use this to determine $\xi(t)$ in a step-by-step fashion, choosing the criterion $C(t_1, t_2) = a$ for $a = 0.3$ to define $\xi(t_2) - \xi(t_1) = \Delta\xi \equiv 1$ (other choices of a yield equivalent results, see the Supplement). The iterative procedure for determining the material time is illustrated in Fig. 3(a) using a linear time axis. Figure 3(b) shows $\xi(t)$ in log-log representation for two temperature jumps, as well as in equilibrium where ξ as mentioned is a linear function of t . In the inset $\xi(t)$ is plotted in linear representation. Figure 3(c) shows the aging rate defined by

$$\gamma \equiv \frac{d\xi}{dt}, \quad (5)$$

which, upon a temperature jump, goes from one value at the shortest times probed to the equilibrium rate at the annealing temperature marked by the horizontal dashed line.

Next we validate the TN prediction that normalized relaxation functions for a given physical quantity following temperature jumps are identical when regarded as functions of the material time ξ [6, 8]. In order to do this, we again consider the time-resolved correlation function of intensity fluctuations $C(t, t + \Delta t)$, this time, however, as a function of time t evaluated at a constant and short lagtime (here $\Delta t = 6\text{ s}$). We write in short $C_{\Delta t}(t)$ and note that, if Δt is chosen in a suitable manner, then $C_{\Delta t}(t)$ represents the change of the fluctuations during aging. In order to obtain a normalized relaxation function $R_{\text{DLS}}(t)$ from $C_{\Delta t}(t)$ we define:

$$R_{\text{DLS}}(t) \equiv \frac{C_{\Delta t}(t) - C_{\Delta t}(t \rightarrow \infty)}{C_{\Delta t}(t=0) - C_{\Delta t}(t \rightarrow \infty)}. \quad (6)$$

Figure 3(d) shows $R_{\text{DLS}}(t)$ as a function of time following 2 K and 4 K temperature down jumps, while Fig. 3(e) plots the same data as functions of the material time. The data collapse nicely in (e), confirming the TN prediction.

Going one step further, if the TN concept were fully valid, the material time determined by using the time evolution of any material property during aging should collapse the relaxation function constructed from any observable monitoring

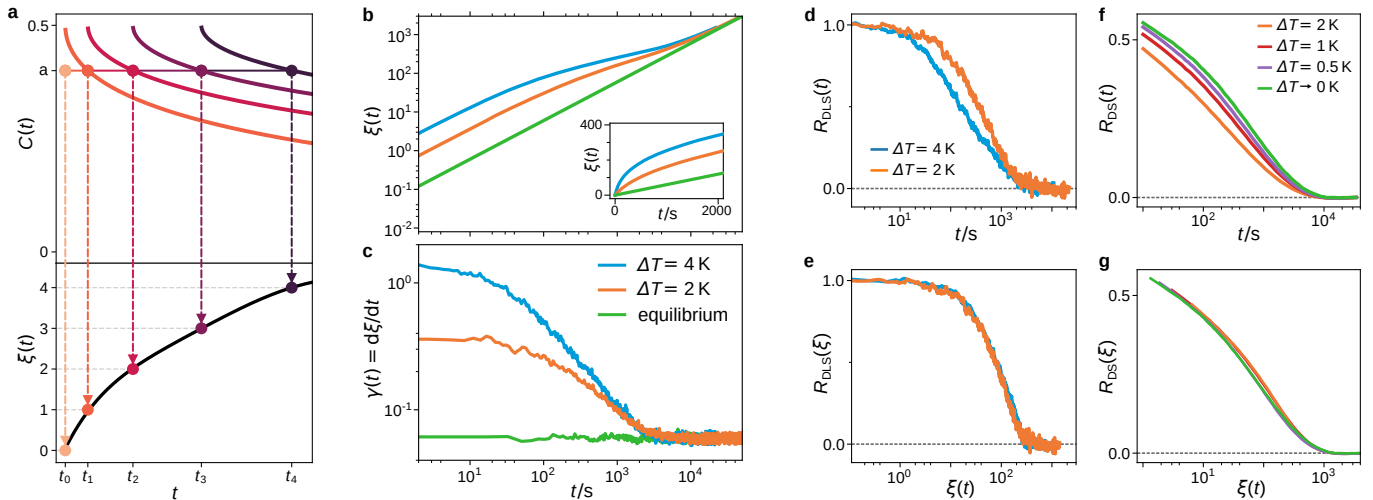


FIG. 3. **Determining and validating the material time for down jumps to 193 K (1P1P data).** (a) Schematic illustration of how ξ is determined step-by-step as a function of the laboratory time t . The time-autocorrelations are plotted on a linear time scale, in contrast to the logarithmic time scale used in Fig. 1. (b) Experimental results of $\xi(t)$ in a logarithmic representation for different temperature jumps and in thermal equilibrium. At short times the samples have only aged insignificantly and $\xi(t)$ is a linear function of time; the same applies in equilibrium which is reached for $t \rightarrow \infty$. The inset shows the same data in linear representation. The 4 K data were adapted to compensate for a slightly different annealing temperature (see the Supplement). (c) The aging rate γ (Eq. (5)) as a function of t . Initially, γ is large because the “material-time clock” ticks fast, but as the aging proceeds γ approaches its equilibrium value. (d) When considered as a function of the laboratory time, due to the fact that aging is nonlinear, the normalized relaxation functions (Eq. (6)) differ in shape for the two temperature jumps. (e) The transformation $t \rightarrow \xi(t)$ collapses the two normalized relaxation functions. (f) Nonlinearity of physical aging is evident also for the normalized relaxation functions of the dielectric loss measured at 10 kHz, $R_{DS}(t)$. The green curve are data for a temperature jump of 0.1 K, which is well within the linear regime. (g) Plotting the dielectric $R_{DS}(t)$ data as functions of the material time leads to the collapse predicted by the TN formalism. Note that the shapes of $R_{DLS}(\xi)$ and $R_{DS}(\xi)$ differ significantly.

the aging process, as the material time would uniquely determine the transient state of the system. To briefly check this rather strong conjecture, Fig. 3(f) shows temperature-jump data for a normalized relaxation function $R_{DS}(t)$ constructed from dielectric loss data $\varepsilon''(\nu, t)$ at the fixed frequency $\nu = 10$ kHz while (g) shows the same data as a function of the material time ξ obtained for the same temperature protocols in the light scattering experiment. As seen in the figure, there is an almost perfect collapse of the data even for $R_{DS}(\xi)$. Considering that the dielectric data were taken in a different laboratory, the observed small deviations are well within the experimental uncertainties. The overall conclusion of panels (d) to (g) is that the TN material time identified from the light-scattering intensity time-autocorrelation function leads to linear behavior when relaxation is considered as a function of the material time, independent of the particular observable used to monitor the aging process. This confirms that the material time has been identified correctly.

V. MATERIAL-TIME STATIONARITY AND REVERSIBILITY

Having shown how to determine the material time during physical aging from the normalized DLS intensity time-autocorrelation function, we now turn to this paper’s central question: Does the linearization obtained by the TN formalism’s replacement of time with material time translate into statistical reversibility of the intensity fluctuations? As mentioned in the Introduction, standard linear-response theory and the Onsager relations embody time reversibility, so it is obvious to investigate the possibility of reversible fluctuations in the material-time description that linearizes the nonlinear physical aging data.

Stationarity of a stochastic process is a necessary condition for reversibility [44]. The top panels of Fig. 4 investigate to which degree the intensity fluctuations are stationary when regarded as functions of the material time for temperature down-jump data taking the system from equilibrium at 197 K to equilibrium at 193 K. Figure 4(a) shows the intensity data as a function of time (blue) and as a function of ξ (red). Although the figures differ visibly, it is not directly clear whether the lower data are more stationary than the upper. To investigate this we determined Fourier components at three different frequencies for fixed-length moving time and material-time windows. The results shown in Fig. 4(b) demonstrate that the material-time description is stationary. Figure 4(c) provides another confirmation

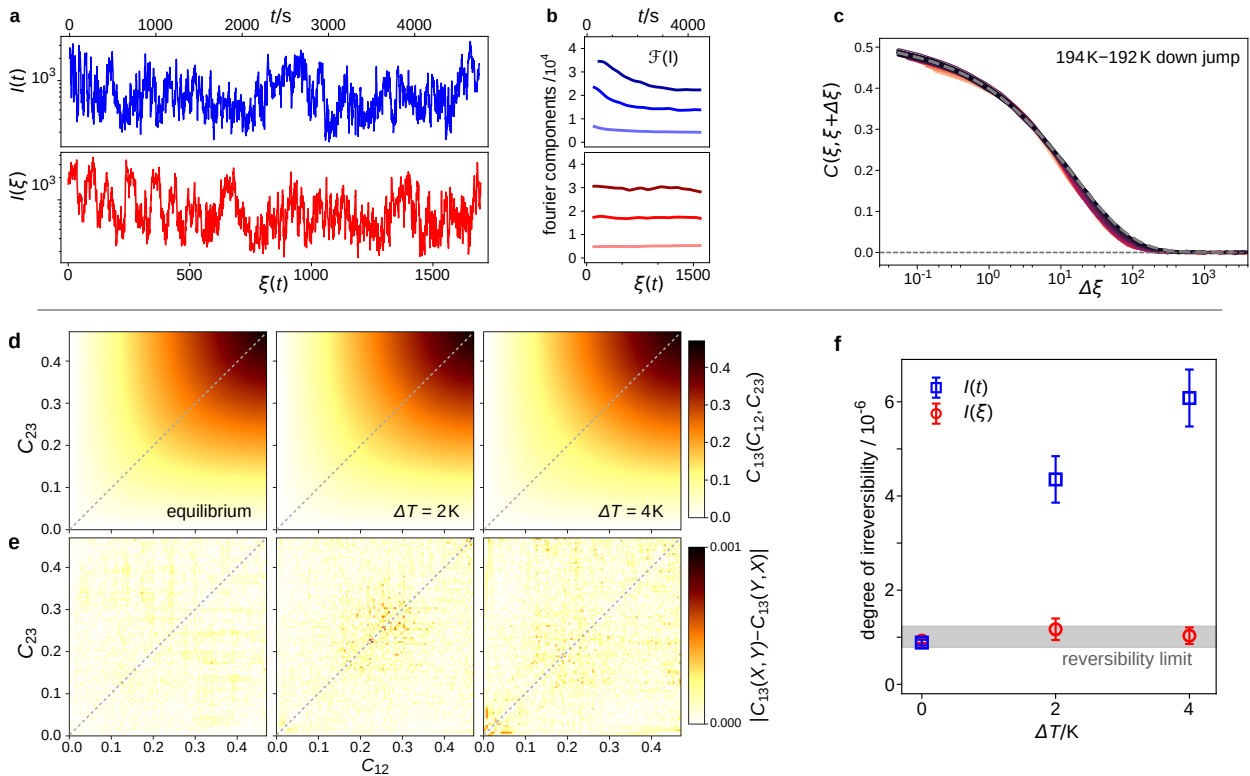


FIG. 4. Stationarity and reversibility of intensity fluctuations regarded as functions of the material time (1P1P data). (a) Light-scattering intensity for a $\Delta T = 4$ K down-jump analyzed at equally spaced time intervals (blue), respectively material-time intervals (red). (b) Moving time-window Fourier components of the intensity at three frequencies plotted as a function of time (upper panel) and material time (lower panel). While a systematic time dependence is observed, the Fourier components are virtually constant as functions of the material time. This shows that fluctuations during physical aging are stationary functions of ξ . (c) shows the autocorrelation functions of Fig. 1 (d) parameterized by the starting material time $\xi(t)$ and plotted as a function of $\Delta\xi(t)$. The data collapse onto one curve, confirming stationarity. (d) shows heat maps of the normalized intensity time-autocorrelation function C_{23} plotted versus C_{12} for fixed values of C_{13} indicated by the colors. Data are given for equilibrium and two temperature down jumps to 193 K. (e) quantifies the deviation from symmetry, $|C_{13}(X, Y) - C_{13}(Y, X)|$, which is in all cases very small. (f) compares the degree of irreversibility for the intensity time series considered as function of t and ξ . The measure used is based on the average visibility-graph degree distributions [41, 42] averaged over 10^4 time series and quantified by the Jensen-Shannon divergence. The larger this quantity is, the more irreversible is the time series in question. Note that zero can only be reached for an infinitely long reversible time series; the gray “reversibility limit” was identified by surrogate data testing [43], which performs the same analysis on a set of artificially generated reversible time series of same statistics and length as the actual data time series (see the Methods section).

of stationarity by demonstrating that $C(\xi, \xi + \Delta\xi)$ is independent of ξ . This is not surprising because stationarity follows from the definition of the material time in conjunction with the triangular relation

After validating stationarity of the $I(\xi)$ time series, the lower panels of Fig. 4 investigate whether reversibility applies in the sense that the time series of intensity fluctuations has the same statistics as that of the time-reversed series. Figure 4(d) shows data for the normalized intensity time-autocorrelation function in equilibrium and for physical aging in a heat map showing $C_{13} \equiv C(t_1, t_3)$ (defined by the colors) as a function of C_{12} and C_{23} . The diagonal symmetry confirms Eq. (3). The degree of deviations from symmetry for given values of $X = C_{12}$ and $Y = C_{23}$, $|C_{13}(X, Y) - C_{13}(Y, X)|$, is investigated in (e) that only shows small deviations. A different test of material-time reversibility is given in (f), where we apply the visibility-graph algorithm [41] to the intensity time series. This algorithm is well suited for our data as it works scale-free and assesses “global” aspects of reversibility [42]. The idea is to map the time series onto a directed graph with nodes representing the time-series element edges defined according to a geometric criterion, *in casu* “visibility” in the sense of how far one can see along the time axis [41]. If a given time series is reversible, the graph thus constructed has the same statistical properties as the time-reversed one. This can be tested by comparing their respective degree distributions using an appropriate statistical measure, e.g., the Jensen-Shannon divergence [45]. Figure 4(f) shows this measure of the degree of irreversibility for the $I(t)$ and $I(\xi)$ fluctuations (blue and red, respectively). The gray area marks the lower range of values that can be obtained for a finite time series, since only an infinite reversible time series has zero Jensen-Shannon divergence. We conclude that,

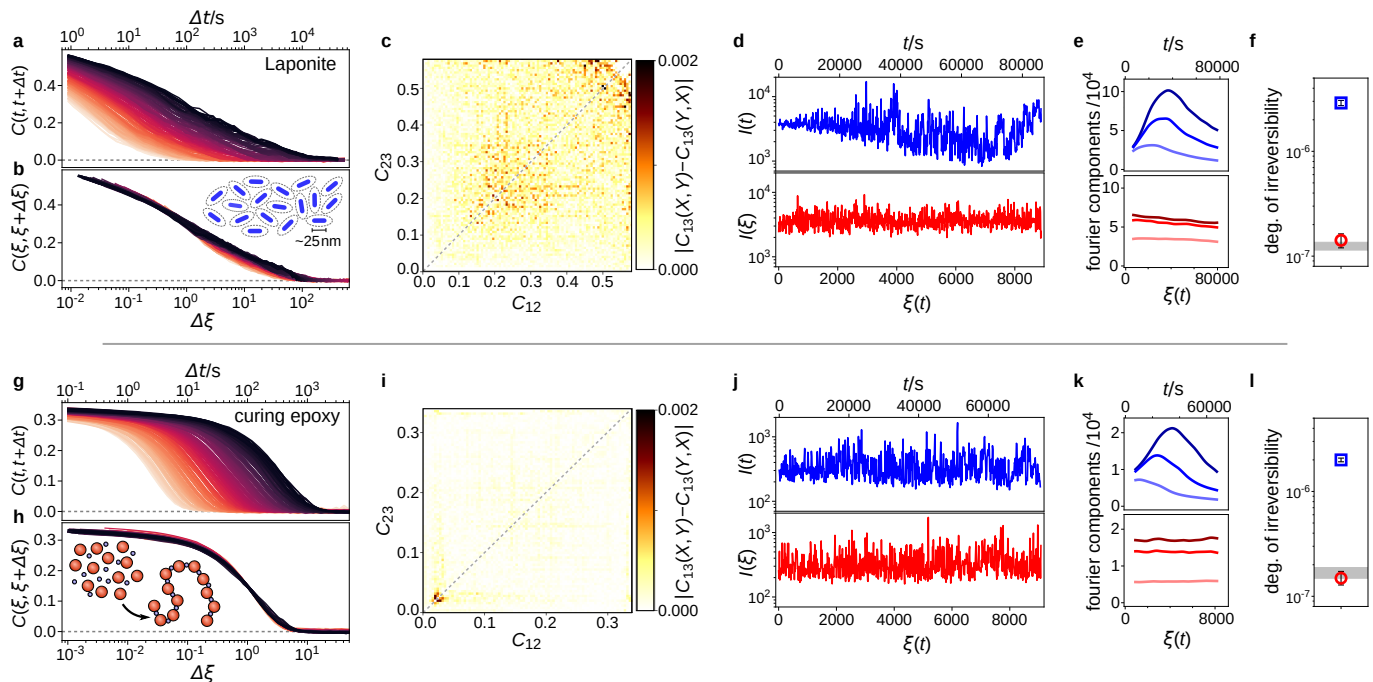


FIG. 5. **Physical aging data for the colloidal glass-former Laponite and chemical aging data for a linear polymerizing epoxy.** The top panels show data for disc-shaped Laponite particles dissolved in deionized water that gradually solidify into a colloidal glass. The bottom panels present the same analysis for the linear polymerization of bisphenol A diglycidyl ether initiated upon mixing with appropriate linker molecules. (a)/(g) show the slow down of time-autocorrelation functions as the annealing time increases. (c)/(i) show heat maps analogous to those of Fig. 4(e), confirming material-time reversal invariance. The necessary condition of stationarity of the intensity time series, shown in (d)/(j), with regard to the material time (red) is confirmed for the corresponding Fourier components in (e)/(k) and for the time autocorrelations in (b)/(h). (f)/(l) shows the test results for time-reversibility analogous to that of Fig. 4(f). By contrast, the intensity fluctuations are not time-reversal invariant when regarded as functions of time (blue)

within the experimental resolution, the physical aging of 1PIP leads to intensity fluctuations of scattered light that are statistically reversible when regarded as functions of the material time.

VI. RESULTS FOR LAPONITE AND A POLYMERIZING EPOXY

To test the generality of the above findings we also investigated Laponite, a colloidal system of synthetic ~ 25 nm sized disc-shaped clay particles that after stirring in water solidifies gradually into a transparent colloidal glass [46]. In this case one cannot probe the approach to equilibrium, because the system keeps solidifying within any realistic time window of observation. Nevertheless, following the above procedure one can define a material time from the normalized scattered-light intensity time-autocorrelation function. In order to further vary the experimental conditions, we changed from VH to the VV light-scattering geometry, which probes local particle-concentration fluctuations [28].

Our results for Laponite are summarized in the top panels of Fig. 5 in which (a) shows the raw data for the normalized intensity time-autocorrelation function. Clearly, the particle dynamics slows down considerably during the experiment. Figure 5(c) confirms the symmetry of $C_{13}(C_{23}, C_{12})$ analogous to Fig. 4(e), a special case of material-time reversibility. Material-time stationarity is illustrated in (b). There is not a perfect data collapse, but it should be noted that these Laponite aging data cover more than two decades of relaxation times. Finally, (d) shows the intensity time and material-time series, (e) shows three of their respective Fourier components evaluated over moving time windows, and (f) demonstrates material-time reversibility following the same procedure as in Fig. 4(f).

Our work set out to investigate whether material-time reversibility is characteristic for *physical* aging. Having confirmed this for two quite different systems, we searched for a counterexample and decided to investigate an irreversibly reacting chemical system namely the linearly polymerizing epoxy based on bisphenol A diglycidyl ether (for details see the Methods section). We monitored the orientational segmental dynamics during polymerization by VH depolarized light scattering. The results are shown in the lower panels of Fig. 5, which is analogous to the representation for Laponite. Surprisingly, the findings are very similar by demonstrating stationarity in (k), collapse of correlation functions in (h), and material-time reversibility in (i) and (l).

VII. DISCUSSION

We have presented aging data for a supercooled molecular liquid obtained by multi-speckle dynamic light scattering. By averaging over a multitude of speckles at a given time, time-resolved intensity autocorrelation functions can be determined with good accuracy during aging. This presents a significant advantage over other experimental approaches that are commonly used to monitor aging dynamics. Our approach allows a detailed analysis of the shape of time-autocorrelation functions during aging even when the time scales of aging and the observed correlation decay are similar.

In the present work we used light-scattering data to validate the material-time concept of the TN formalism. This has been used successfully for half a century to describe physical aging [6, 8, 12, 16] and is remarkable by transforming a highly nonlinear phenomenon into a linear one simply by replacing time with material time. As argued in the introduction, since standard linear-response theory reflects the time reversibility of the fundamental laws of physics, this suggests that fluctuations during physical aging are statistically reversible when regarded as functions of the material time. We have validated this for light-scattering data on three aging systems: 1-phenyl-1-propanol (1P1P), Laponite, and a curing epoxy. These systems are quite different: 1P1P and epoxy are molecular while Laponite is colloidal; 1P1P and Laponite age physically while epoxy ages chemically; Laponite and epoxy do not converge to equilibrium within our window of observation while 1P1P does. Moreover, 1P1P and epoxy were studied in the VH light-scattering geometry probing orientational fluctuations whereas the VV geometry probing density fluctuations was applied in the study of Laponite aging. Despite these differences, all three systems obey the triangular relation Eq. (2) and have fluctuations that are stationary and reversible when considered as functions of the material time.

Although there have been a number of attempts to compare aging behavior monitored by different experimental methods [8, 12], the following question arises in the context of the TN formalism: Does the material time determined by one specific method, say DLS, uniquely determine the transient state of the aging system? That is, does any other observable that probes the aging process become linear and the corresponding fluctuations stationary and time reversible when considered as function of that particular material time? We made a first attempt to elucidate this questions by showing that relaxation functions constructed from dielectric data indeed do become linear using the DLS material time. Whether this holds in general and includes other static and dynamic observables so far remains an open question. We note that results from different linear-response experiments show that, at least for some glass-forming liquids, the ratio of different relaxation times is independent of the temperature [47], which is a necessary condition for a unique material time to exist.

While the concept of reversibility is fundamental in physics, it is discussed much more generally as a time-series property, e.g., very recently in connection with neuroscience [48]. We are not aware of a theoretical framework that predicts material-time statistical reversibility of fluctuations during aging. The TN formalism is known to work best for physical aging relatively close to equilibrium, i.e., involving small albeit still strongly nonlinear temperature variations [8, 12]. This aging description is phenomenological and has no predictions for fluctuations. Assuming in the TN spirit that the intensity time-autocorrelation function during aging is a function of the material time increase, the triangular relation Eq. (2) and the symmetry relation Eq. (3) were derived above; in that approach these identities are inherited from thermal equilibrium. Equation (2) and Eq. (3) were originally derived, however, by Cugliandolo and Kurchan (CK) in an entirely different context [30, 49]. CK studied spin models with infinite-range interactions and showed that the exact Schwinger-Dyson equations for fluctuation and response imply Eq. (2) and Eq. (3) below a phase-transition temperature where the system never converges to equilibrium. Above the phase transition temperature, on the other hand, where the system converges to equilibrium no triangular relation is predicted to apply. Under the latter conditions, however, the triangular relation do apply as shown above for 1P1P and in computer simulations of simple Lennard-Jones type systems aging to equilibrium [39, 40]. The CK mean-field approach provides an exact description of aging in infinite dimensions [30, 50]. Although the basic CK predictions were later proposed to apply also in finite dimensions [39, 51], the range of applicability of the CK mean-field scenario remains unclear [15]. Interestingly, the subject of time-reparametrization invariance has recently become fashionable in field theory where it represents the “gravity” low-energy limit [52, 53].

Our results give rise to a number of general questions: Is material-time reversibility a universal characteristic of aging and, if so, does the same material time lead to reversibility of different fluctuating quantities? Does material-time reversibility somehow reflect the reversibility of the fundamental laws of physics? In particular: Is there a connection to the fluctuation theorem that quantifies the consequences of microscopic time reversibility [54, 55]? – To illuminate these questions it would be interesting to find an ageing system that violates material-time reversibility, but we have so far failed to do so.

VIII. METHODS: EXPERIMENTAL PROCEDURE AND DATA ANALYSIS

A. Multispeckle DLS setup and temperature protocols

Experiments are performed in a custom-built light-scattering setup, where a Cobolt Samba 500 Nd:YAG laser is used to illuminate the sample with vertically polarized light. The sample cell is mounted inside a Cryovac cold-finger cryostat and is surrounded by high vacuum generated by a vibration-free Agilent ion getter pump. Scattered light is detected at 90° angle using a Hamamatsu ORCA-Flash 4.0 V2 sCMOS camera. Light is guided onto the camera chip by a custom-built optical system consisting of a circular aperture, a $f = 6$ cm spherical lens, a fine-adjustable Glan-Thompson polarizer from B. Halle with extinction ratio 10^{-6} , an adjustable slit aperture, and finally a 2 nm band-pass filter in the respective order towards the detection unit. The scattering volume and the slit aperture are located at the two focal points of the lens, respectively.

To calibrate the temperature protocols, the sample temperature had to be monitored precisely. This was achieved by constructing a dummy sample cell, which has the same geometry as the original light-scattering cell, but is equipped with two PT100 temperature sensors: The first one is located inside the liquid sample, the second one is glued into a channel drilled through the aluminum bottom of the sample cell using Loctite Stycast 2850FT thermally conducting epoxy glue. During the light-scattering measurements, only the second sensors could be used, as positioning a sensor inside the liquid would interfere with the laser beam. Using the dummy sample cell it was confirmed that both sensors coincide by checking different temperature protocols.

To perform a fast temperature down jump from $T_0 = 197$ K, 195 K to $T_\infty = 193$ K with amplitude $\Delta T = T_0 - T_\infty$ it is insufficient to simply quench the cold-finger from T_0 to T_∞ and to let the sample equilibrate afterwards. Due to the thermal lag between cold-finger and sample cell, the sample temperature would initially decrease quickly, but as soon as the cold-finger reaches T_∞ , the cooling rate inside the sample declines and it takes > 1000 s for the sample temperature to reach T_∞ . As a solution we initially undercooled the cold-finger to several degrees below T_∞ as quickly as possible. This temperature was then held for a short time t , after which the cold finger was heated back to T_∞ with heating rate c . By choosing the parameters t and c in an optimal way, it was possible to ensure that the sample temperature quickly reached T_∞ without any significant temperature undershoot (see SI for details). The parameters for such an optimal temperature protocol were determined for $\Delta T = 2.0$ and 4.0 K prior to the light-scattering measurements. During the measurements, the prepared temperature protocols were repeated, where reproducibility was ensured by controlling the Lakeshore 335 temperature controller via python scripts. Following this procedure, temperature jumps could be performed in < 200 s with an accuracy of 0.1 K. The final temperature can then be held for > 24 h with an accuracy of ± 0.05 K.

B. Sample preparation and measurements

1. 1P1P

1-phenyl-1-propanol (1P1P; Alfa Aesar, 98+% purity) was filtered into the light-scattering sample cell using a 450 nm syringe filter. The sample was first kept at T_0 for 12 h to ensure the supercooled liquid is in (metastable) thermal equilibrium. Subsequently, a camera measurement quantifying the equilibrium state at T_0 was performed with exposure time 0.02 s over 300,000 frames (6000 s). After this, a second camera measurements was started with an exposure time of 0.2 s over 300,000 frames (~ 17 h). Simultaneously, the prepared temperature protocol was initiated. All experiments involving 1P1P were performed in the VH (depolarized) geometry, thus the reorientation of the molecular optical anisotropy tensor is probed[28].

For the dielectric measurements the complex capacity was measured at a fixed frequency, $\nu_0 = 10$ kHz, with an Andeen-Hagerling AH 2700A high precision bridge in a custom-built cryostat system [56, 57]. Fast temperature jumps up to $\Delta T = 4$ K with microkelvin precision are obtained by a subcryostat system based on a Peltier element and a nonlinear temperature sensor [56, 58]. By this, the sample temperature can be changed in a few seconds.

The dielectric constant of 1-phenyl-1-propanol was measured at 10 kHz and the dielectric aging function, $R_{DS}(t)$, was calculated from the imaginary part of the complex permittivity at this frequency, ϵ'' , (analogous to Equation (6))

$$R_{DS}(t) = \frac{\epsilon''(t) - \epsilon''(t \rightarrow \infty)}{\epsilon''(t=0) - \epsilon''(t \rightarrow \infty)} \quad (7)$$

where $t = 0$ refers to the equilibrium value before the jump. The dielectric aging function is thus normalized to the difference in the equilibrium values at the start and the end temperature for the temperature jump. Data were collected linearly in time and averaged using a logarithmic binning scheme. For combining DLS and DS measurements

we account for slight differences regarding annealing temperature that inevitably appear due to the experiments being performed in different laboratories. We determine the respective relaxation time at the annealing temperatures of both experiments by considering the results from a detailed analysis of 1P1P in both methods in Ref. [59] and, finally, apply the procedure presented in S1 of the Supplementary Information to consider the temperature difference.

2. Laponite

The Laponite suspension was prepared in consideration of the phase diagram [60] with parameters chosen such that a colloidal Wigner glass was obtained: Laponite powder (Laponite-RD from BYK) was dried for one week at 1 mbar to remove any water content. Water with pH 10 and ionic strength $I < 10^{-4}$ M was obtained by adding an appropriate amount of NaOH to milli-Q water. Subsequently, 2.98 wt% of Laponite was added and the mixture was stirred for 24 h. Finally, the sample was filtered into a glass cylinder using a 450 nm syringe filter. Filtration might have led to a slight reduction of the Laponite concentration. Physical aging starts directly after the mixture is filtered, however, for the first few hours the colloidal dynamics is too fast to be captured by the camera. The camera measurement with exposure time 0.1 s was started several minutes after filtration and the scattered light was monitored in VV (polarized) geometry over 1,500,000 frames (~ 42 h). Laponite was studied at room temperature.

3. Epoxy

The epoxy system is based on bisphenol A diglycidyl ether resin (Alfa Aesar). As polymerization agent we used N,N,N',N'-tetraethyldiethylenetriamine (Sigma Aldrich, 90%). This specific agent induces a linear polymerization, thus, the mixture was prepared with a 1:1 molar ratio. Before mixing, the resin was dried and degassed in a vacuum oven. Afterwards, it was filled into a glass syringe equipped with a stainless steel filter holder containing a 450 nm nylon membrane filter suitable for operation at high temperatures. The syringe was then heated to 150 °C to decrease the viscosity of the resin, which allowed us to filter the resin into a dust-free sample glass. The appropriate amount of hardener was added, again, using a syringe filter. Subsequently, the mixture was magnetically stirred at 400 rpm for 10 min and filled into a dust-free cylindrical glass sample holder. Air-bubbles were removed by exposing the mixture to vacuum for 15 min. Finally, the glass tube was sealed and placed inside a suitable sample oven, which had been preheated to 310 K, and the camera measurement in VH geometry with exposure time 0.1 s was started for 2,000,000 frames (~ 56 h).

C. Data analysis

For all performed temperature jumps of 1P1P, for laponite during annealing and for the curing epoxy, the resulting camera movie files were analyzed using three different techniques to obtain time-resolved auto-correlation functions, pair-wise auto-correlations for time triplets, and intensity time-series (TS) as function of time t and material time ξ . In the following, each procedure and subsequent analyses are explained independently.

1. Time-resolved auto-correlation functions

Time-resolved auto-correlation functions were obtained from the camera movie via a multi-pixel average over images consisting of $N = 2048$ columns and $M = 350$ rows. Due to the Gaussian intensity profile of the laser beam, average pixel intensities slightly vary perpendicular to the propagation direction of the laser (res. for different rows). At the same time, the average intensity is constant along the propagation direction (res. for different columns). Thus, normalization of auto-correlations is carried out independently for each row and finally, the result is averaged over all rows:

$$C(t, t + \Delta t) = \frac{1}{M} \sum_{j=1}^M \left[\frac{\sum_{i=1}^N I_{ij}(t) I_{ij}(t + \Delta t)}{\left(\sum_{i=1}^N I_{ij}(t)\right) \left(\sum_{i=1}^N I_{ij}(t + \Delta t)\right)} \right] - 1, \quad (8)$$

with column i and row j . $C(t, t + \Delta t)$ was calculated for all available t (each frame) and for 47 different logarithmically spaced values of Δt , where the smallest value is chosen as equal to the exposure time of the camera.

2. Pair-wise auto-correlation for time triplets

In order to verify triangular relation (Equation (2)), we analyzed numerous time triplets $t_1 < t_2 < t_3$. Analysis focused on the time frame where $\gamma(t)$ changes, as triangular relation holds trivially when $\gamma(t) = \text{const}$. In this time frame, 10^3 linearly spaced values of t_1 were chosen. For each t_1 , different $t_2 = t_1 + \tau'$ were constructed for 169 logarithmically spaced values τ' . Subsequently, for each combination of t_1 and t_2 , different $t_3 = t_2 + \tau''$ were constructed using the same 169 logarithmically spaced values for τ'' . Combined, this procedure generated $1000 \cdot 169^2 = 28.561 \cdot 10^6$ different time triplets. For each of these triplets the pairwise auto-correlations C_{12} , C_{13} and C_{23} (see main text for notation) were calculated using equation (8) (with e.g. $t = t_1$ and $t + \tau = t_2$ for the calculation of C_{12}). Finally, subsets with (almost) the same values of C_{12} and C_{23} were binned (with resolution $\Delta C = 0.005$) and for each subset the mean $\overline{C_{13}}(C_{12}, C_{23})$ and the corresponding standard deviation $\sigma_{13}(C_{12}, C_{23})$ was calculated.

3. Constructions of intensity TS

To obtain intensity TS in laboratory time $I(t)$, res. material time $I(\xi)$, intensity fluctuations in one pixel were first interpolated at a tightly spaced list of times, where the elapsed time between consecutive points was chosen to be constant in time, res. material time. As the focus is on physical aging, the analysis is limited to the time frame where $\gamma(t)$ changes (same time-frame as for time triplets). Afterwards, subsets were binned and averaged to obtain TS of length $N \in \{500, 1000, 2500, 5000, 10000\}$. For $I(\xi)$, this procedure essentially simulates the result one would obtain using a camera operated with a time-dependent exposure time according to the material time-clock rate. Different N were analyzed to ensure observed effects are universal regarding temporal resolution. As qualitatively equivalent results were obtained for all N , only $N = 2500$ is shown in this paper. The above described procedure was applied 10^4 different pixels, chosen such that fluctuations are statistically independent. The entire subset is then analyzed regarding stationarity and reversibility.

4. TS stationarity analysis

In addition to the analysis of auto-correlations as a function of time and material time, stationarity was analyzed for $I(t)$ and $I(\xi)$ by calculating the local Fourier transform. First, the TS was multiplied by a Gaussian with varying maximum position t , res. ξ , and a standard deviation of 100 time-steps. The thereby obtained TS contains time-resolved information of the original TS around time t , res. material time ξ . Finally, for different t , res. ξ , the Fast Fourier transform (FFT) algorithm was applied and the result was averaged over 10^4 statistically independent TS. In Figs. 4 and 5 selected Fourier components are plotted as a function of t res. ξ .

5. TS time-reversibility analysis

Time-reversibility of $I(t)$ and $I(\xi)$ was analyzed using the visibility graph (VG) algorithm [41, 42]. This was done by transforming a TS $I(t)$ res. $I(\xi)$ and its respective time-invert $I^-(t)$ res. $I^-(\xi)$ into a VG using the fast algorithm [61] from the TS2VG python package. Subsequently their respective degree distributions were calculated. Finally, the obtained degree distributions of original and time-inverted TS, $P(k)$ and $P^-(k)$, were averaged over 10^4 statistically independent TS and the difference of both distributions was quantified using the Jensen-Shannon divergence

$$D_{\text{JS}}(P(k)||P^-(k)) = \frac{1}{2} \left(D_{\text{KL}}(P(k)||\tilde{P}(k)) + D_{\text{KL}}(P^-(k)||\tilde{P}(k)) \right), \quad (9)$$

where $\tilde{P}(k) = \frac{1}{2}(P(k) + P^-(k))$ and

$$D_{\text{KL}}(P(k)||\tilde{P}(k)) = \sum_k P(k) \log \frac{P(k)}{\tilde{P}(k)} \quad (10)$$

is the Kullback-Leibler divergence. D_{JS} can be thought of as the symmetric version of D_{KL} and is descriptively referred to as *degree of irreversibility* in the paper.

Error bars for D_{JS} were determined by repeating the above described analysis ten times for different subsets of 10^4 pixels (no pixel was used in more than one subset). The standard deviations of the thus obtained distributions of D_{JS} are plotted as error bars in Figs. 4 and 5.

Due to finite size effects, $D_{JS} > 0$ even for truly time-reversible TS of *finite* length. To obtain the lower limit of D_{JS} that would be approached if experimentally observed TS were truly time-reversible, we performed a surrogate analysis[43]. Numerous surrogate TS of $I(\xi)$ and $I^-(\xi)$ were calculated using the Iterated Amplitude Adjusted Fourier Transform (iAAFT) algorithm[62] and analyzed in subsets of 10^4 TS (equivalent to the procedure of analyzing experimental TS). The reversibility limit in Figs. 4 and 5 corresponds to the distribution of D_{JS} obtained by performing several of such surrogate analyses.

SI CONTENTS

Temperature protocol and handling slight temperature differences, influence of the parameter a on the material time and more details regarding the statistical analysis of reversibility

ACKNOWLEDGMENTS

The authors thank Massimiliano Zanin and Susanne Ditlevsen for advice regarding the data analysis. This work was supported by the VILLUM Foundation's *Matter* grant (16515) and by the Deutsche Forschungsgemeinschaft (grant no. BL 1192/3).

-
- [1] C. Rovelli, *The Order of Time* (Penguin Books, 2018).
- [2] L. D. Landau and E. M. Lifshitz, *Statistical Physics* (Pergamon, Oxford, 1958).
- [3] L. E. Reichl, *A Modern Course in Statistical Physics*, 4th ed. (Wiley-VCH, 2016).
- [4] L. Onsager, Reciprocal relations in irreversible processes. II., *Phys. Rev.* **38**, 2265 (1931).
- [5] A. Q. Tool, Relation between inelastic deformability and thermal expansion of glass in its annealing range, *J. Amer. Ceram. Soc.* **29**, 240 (1946).
- [6] O. S. Narayanaswamy, A model of structural relaxation in glass, *J. Amer. Ceram. Soc.* **54**, 491 (1971).
- [7] L. C. E. Struik, *Physical Aging in Amorphous Polymers and Other Materials* (Elsevier, Amsterdam, 1978).
- [8] G. W. Scherer, *Relaxation in Glass and Composites* (Wiley, New York, 1986).
- [9] I. M. Hodge, Physical aging in polymer glasses, *Science* **267**, 1945 (1995).
- [10] K. Chen and K. S. Schweizer, Molecular theory of physical aging in polymer glasses, *Phys. Rev. Lett.* **98**, 167802 (2007).
- [11] M. Micoulaut, Relaxation and physical aging in network glasses: a review, *Rep. Prog. Phys.* **79**, 066504 (2016).
- [12] G. B. McKenna and S. L. Simon, 50th anniversary perspective: Challenges in the dynamics and kinetics of glass-forming polymers, *Macromolecules* **50**, 6333 (2017).
- [13] B. Ruta, E. Pineda, and Z. Evenson, Relaxation processes and physical aging in metallic glasses, *J. Phys.: Condens. Mat.* **29**, 503002 (2017).
- [14] D. Cangialosi, Physical aging of polymers, in *Encyclopedia of Polymer Science and Technology* (2018) pp. 1–36.
- [15] F. Arceri, F. P. Landes, L. Berthier, and G. Biroli, Glasses and aging: A statistical mechanics perspective, arXiv:2006.09725 (2020).
- [16] G. B. McKenna, On the physics required for prediction of long term performance of polymers and their composites, *J. Res. Natl. Inst. Stand. Technol.* **99**, 169 (1994).
- [17] X. Monnier, D. Cangialosi, B. Ruta, R. Busch, and I. Gallino, Vitrification decoupling from α -relaxation in a metallic glass, *Sci. Adv.* **6**, eaay1454 (2020).
- [18] Y. Zhao, B. Shang, B. Zhang, X. Tong, H. Ke, H. Bai, and W.-H. Wang, Ultrastable metallic glass by room temperature aging, *Sci. Adv.* **8**, eabn3623 (2022).
- [19] F. Simon, Über den Zustand der unterkühlten Flüssigkeiten und Gläser, *Z. Anorg. Allg. Chem.* **203**, 219 (1931).
- [20] C. B. Roth, ed., *Polymer Glasses* (CRC Press (Boca Raton, FL, USA), 2017).
- [21] M. Lulli, C.-S. Lee, H.-Y. Deng, C.-T. Yip, and C.-H. Lam, Spatial heterogeneities in structural temperature cause Kovacs' expansion gap paradox in aging of glasses, *Phys. Rev. Lett.* **124**, 095501 (2020).
- [22] R. Mandal and P. Sollich, Multiple types of aging in active glasses, *Phys. Rev. Lett.* **125**, 218001 (2020).
- [23] R. Pastore, C. Siviello, and D. Larobina, Elastic and dynamic heterogeneity in aging alginate gels, *Polymers* **13**, 3618 (2021).
- [24] G. Janzen and L. M. C. Janssen, Aging in thermal active glasses, *Phys. Rev. Res.* **4**, L012038 (2022).
- [25] H. R. Schober, Diffusion, relaxation, and aging of liquid and amorphous selenium, *Phys. Rev. B* **103**, 094202 (2021).
- [26] A. J. Kovacs, J. J. Aklonis, J. M. Hutchinson, and A. R. Ramos, Isobaric volume and enthalpy recovery of glasses. II. A transparent multiparameter theory, *J. Polym. Sci. Polym. Phys.* **17**, 1097 (1979).
- [27] B. Riechers, L. A. Roed, S. Mehri, T. S. Ingebrigtsen, T. Hecksher, J. C. Dyre, and K. Niss, Predicting nonlinear physical aging of glasses from equilibrium relaxation via the material time, *Sci. Adv.* **8**, eabl9809 (2022).
- [28] B. J. Berne and R. Pecora, *Dynamic Light Scattering: With Applications to Chemistry, Biology, and Physics* (Wiley, 1976).

- [29] B. Riechers and R. Richert, Rate exchange rather than relaxation controls structural recovery, *Phys. Chem. Chem. Phys.* **21**, 32 (2019).
- [30] L. F. Cugliandolo and J. Kurchan, On the out-of-equilibrium relaxation of the Sherrington-Kirkpatrick model, *J. Phys. A: Math. Gen.* **27**, 5749 (1994).
- [31] V. Viasnoff and F. Lequeux, Rejuvenation and overaging in a colloidal glass under shear, *Phys. Rev. Lett.* **89**, 065701 (2002).
- [32] L. Cipelletti, H. Bissig, V. Trappe, P. Ballesta, and S. Mazoyer, Time-resolved correlation: a new tool for studying temporally heterogeneous dynamics, *J. Phys.: Condens. Matter* **15**, S257 (2002).
- [33] S. Kaloun, M. Skouri, A. Knaebel, J.-P. Münch, and P. Hébraud, Aging of a colloidal glass under a periodic shear, *Phys. Rev. E* **72**, 011401 (2005).
- [34] Q. Li, X. Peng, and G. B. McKenna, Long-term aging behaviors in a model soft colloidal system, *Soft Matter* **13**, 1396 (2017).
- [35] S. Aime, L. Ramos, and L. Cipelletti, Microscopic dynamics and failure precursors of a gel under mechanical load, *PNAS* **115**, 3587 (2018).
- [36] B. Ruta, Y. Chushkin, G. Monaco, L. Cipelletti, E. Pineda, P. Bruna, V. M. Giordano, and M. Gonzalez-Silveira, Atomic-scale relaxation dynamics and aging in a metallic glass probed by X-ray photon correlation spectroscopy, *Phys. Rev. Lett.* **109**, 165701 (2012).
- [37] Z. Evenson, B. Ruta, S. Hechler, M. Stolpe, E. Pineda, I. Gallino, and R. Busch, X-ray photon correlation spectroscopy reveals intermittent aging dynamics in a metallic glass, *Phys. Rev. Lett.* **115**, 175701 (2015).
- [38] A. Cornet, G. Garbarino, F. Zontone, Y. Chushkin, J. Jacobs, E. Pineda, T. Deschamps, S. Li, A. Ronca, J. Shen, G. Morard, N. Neuber, M. Frey, R. Busch, I. Gallino, M. Mezouar, G. Vaughan, and B. Ruta, Denser glasses relax faster: a competition between rejuvenation and aging during in-situ high pressure compression at the atomic scale, arXiv: , 2301.02551 (2023).
- [39] K. E. Avila, H. E. Castillo, and A. Parsaeian, Fluctuations in the time variable and dynamical heterogeneity in glass-forming systems, *Phys. Rev. E* **88**, 042311 (2013).
- [40] I. M. Douglass and J. C. Dyre, Distance-as-time in physical aging, *Phys. Rev. E* **106**, 054615 (2022).
- [41] L. Lacasa, B. Luque, F. Ballesteros, J. Luque, and J. C. Nuno, From time series to complex networks: The visibility graph, *PNAS* **105**, 4972 (2008).
- [42] L. Lacasa, A. Nunez, E. Roldán, J. M. R. Juan, and B. Luque, Time series irreversibility: a visibility graph approach, *Eur. Phys. J. B* **85**, 1 (2012).
- [43] T. Schreiber and A. Schmitz, Surrogate time series, *Physica D* **142**, 346 (2000).
- [44] A. J. Lawrance, Directionality and reversibility in time series, *Int. Stat. Rev.* **59**, 67 (1991).
- [45] M. L. Menéndez, J. A. Pardo, L. Pardo, and M. C. Pardo, The Jensen-Shannon divergence, *J. Franklin Inst.* **334**, 307 (1997).
- [46] B. Ruzicka and E. Zaccarelli, A fresh look at the Laponite phase diagram, *Soft Matter* **7**, 1268 (2011).
- [47] L. A. Roed, J. C. Dyre, K. Niss, T. Hecksher, and B. Riechers, Time-scale ordering in hydrogen- and van der Waals-bonded liquids, *J. Chem. Phys.* **154**, 184508 (2021).
- [48] M. L. Kringelbach, Y. S. Perl, E. Tagliazucchi, and G. Deco, Toward naturalistic neuroscience: Mechanisms underlying the flattening of brain hierarchy in movie-watching compared to rest and task, *Sci. Adv.* **9**, eade6049 (2023).
- [49] C. Chamon and L. F. Cugliandolo, Fluctuations in glassy systems, *J. Stat. Mech.* **7**, P07022 (2007).
- [50] E. Agoritsas, T. Maimbourg, and F. Zamponi, Out-of-equilibrium dynamical equations of infinite-dimensional particle systems I. The isotropic case, *J. Phys. A: Math. Theor.* **52**, 144002 (2019).
- [51] H. E. Castillo and A. Parsaeian, Local fluctuations in the ageing of a simple structural glass, *Nat. Phys.* **3**, 26 (2007).
- [52] D. Facchetti, G. Biroli, J. Kurchan, and D. R. Reichman, Classical glasses, black holes, and strange quantum liquids, *Phys. Rev. B* **100**, 205108 (2019).
- [53] J. Kurchan, Time-reparametrization invariances, multithermalization and the Parisi scheme, *SciPost Phys. Core* **6**, 001 (2023).
- [54] G. N. Bochkov and Y. E. Kuzovlev, Nonlinear fluctuation-dissipation relations and stochastic models in nonequilibrium thermodynamics. I. Generalized fluctuation-dissipation theorem, *Physica A* **106**, 443 (1981).
- [55] D. J. Evans and D. J. Searles, The fluctuation theorem, *Adv. Phys.* **51**, 1529 (2002).
- [56] B. Igarashi, T. Christensen, E. H. Larsen, N. B. Olsen, I. H. Pedersen, T. Rasmussen, and J. C. Dyre, A cryostat and temperature control system optimized for measuring relaxations of glass-forming liquids, *Rev. Sci. Instrum.* **79**, 045105 (2008).
- [57] B. Igarashi, T. Christensen, E. H. Larsen, N. B. Olsen, I. H. Pedersen, T. Rasmussen, and J. C. Dyre, An impedance-measurement setup optimized for measuring relaxations of glass-forming liquids, *Rev. Sci. Instrum.* **79**, 045106 (2008).
- [58] T. Hecksher, N. B. Olsen, K. Niss, and J. C. Dyre, Physical aging of molecular glasses studied by a device allowing for rapid thermal equilibration, *J. Chem. Phys.* **133**, 174514 (2010).
- [59] T. Böhmer, J. P. Gabriel, T. Richter, F. Pabst, and T. Blochowicz, Influence of molecular architecture on the dynamics of h-bonded supramolecular structures in phenyl-propanols, *J. Phys. Chem. B* **123**, 10959 (2019).
- [60] H. Tanaka, J. Meunier, and D. Bonn, Nonergodic states of charged colloidal suspensions: Repulsive and attractive glasses and gels, *Phys. Rev. E* **69**, 031404 (2004).
- [61] X. Lan, H. Mo, S. Chen, Q. Liu, and Y. Deng, Fast transformation from time series to visibility graphs, *Chaos* **25**, 083105 (2015).
- [62] T. Schreiber and A. Schmitz, Improved surrogate data for nonlinearity tests, *Phys. Rev. Lett.* **77**, 635 (1996).